Differential Behavior of Photoactivated Microtubules in Growing Axons of Mouse and Frog Neurons

Shigeo Okabe and Nobutaka Hirokawa

Department of Anatomy and Cell Biology, School of Medicine, University of Tokyo, Hongo, Tokyo, 113 Japan

Abstract. To characterize the behavior of axonal microtubules in vivo, we analyzed the movement of tubulin labeled with caged fluorescein after activation to be fluorescent by irradiation of 365-nm light. When mouse sensory neurons were microinjected with caged fluorescein-labeled tubulin and then a narrow region of the axon was illuminated with a 365-nm microbeam, photoactivated tubulin was stationary regardless of the position of photoactivation. We next introduced caged fluorescein-labeled tubulin into *Xenopus* embryos and nerve cells isolated from injected embryos were analyzed by photoactivation. In this case, movement of the photoactivated zone toward the axon tip was frequently observed. The photoactivated microtubule segments in the *Xenopus* axon moved out from their initial position without significant spreading, suggesting that fluorescent microtubules are not sliding as individual filaments, but rather translocating en bloc.

Since these observations raised the possibility that the mechanism of nerve growth might differ between two types of neurons, we further characterized the movement of another component of the axon structure, the plasma membrane. Analysis of the position of polystyrene beads adhering to the neurites of *Xenopus* neurons revealed anterograde movement of the beads at the rate similar to the rate of microtubule movement. In contrast, no movement of the beads relative to the cell body was observed in mouse sensory neurons. These results suggest that the mode of translocation of cytoskeletal polymers and some components of the axon surface differ between two neuron types and that most microtubules are stationary within the axon of mammalian neurons where the surface-related motility of the axon is not observed.

THERE is now increasing evidence to suggest that the formation and maintenance of the neuronal cytoskeleton is a major intrinsic determinant of the neuron shape (9, 12, 17–19, 22). Microtubules (MTs)[1] are the main cytoskeletal component in the axon during the process of development and regeneration of the nervous system (54) and studies using antimicrotubular agents have shown that MT depolymerization inhibits neurite elongation (11, 29). These observations indicate that the net increase of tubulin molecules and local MT formation are required for axonal growth (35).

Tubulin molecules necessary for the construction of new axons are known to be synthesized in the cell body and transported down the axon (7, 20, 53). To understand the molecular mechanism of nerve growth, it is necessary to determine the sites of MT assembly and the form by which tubulin subunits are transported. Despite much prior work, the physical state of tubulin during transport is still problematic (21).

Previous radiolabeling studies of axonal transport have shown the similar transport velocity of tubulin and neurofilament proteins (7, 20) and provided the first hypothesis that cytoskeletal polymers are assembled at the cell body and then transported as a cross-linked matrix through the axon. Since detailed analysis on the transport of radiolabeled cytoskeletal proteins in the axon revealed that the velocities and distribution of cytoskeletal proteins are highly variable between different types of neurons (33, 36, 39, 50). This hypothesis was revised to the "polymer sliding" model, which holds that the transport proteins are in the form of individual sliding polymers interacting weakly with other cytoskeletal components (26).

Alternatively, MTs could be stationary in the axon and tubulin subunits themselves or oligomers are the units of transport (21, 41). Our previous study using microinjection of biotinylated tubulin into nerve cells has shown that MTs in neuronal processes continue to turnover and incorporate new tubulin subunits at their distal ends (40). This observation suggests the presence of free tubulin molecules exchanging with polymeric ones locally within the axon. Furthermore, the movement of MTs in the axon was directly monitored by the combination of microinjection of fluorescently labeled tubulin and successive laser photobleaching (30, 31, 43). When fluorescent MTs in the axon of mouse and chick neurons were photobleached, the bleached zone did not move but fluorescence recovered with time. These observations support the idea that most MTs are stationary but dynamic in the axons.

1. *Abbreviations used in this paper*: CCD, charged-coupled device; DIC, differential interference contrast; DRG, dorsal root ganglion; MT, microtubule.

Although fluorescence recovery after photobleaching has been used as a powerful tool for the study of dynamic behavior of biological structures, a new technique of photoactivation of caged fluorescence has been applied to the analysis of dynamic behavior of cytoskeletal polymers (34). Since the photoactivation experiments revealed poleward flux of MTs, which was not detected by the previous reports using the photobleaching method (15), it has been claimed that the photobleaching study might affect the motile processes involving MTs, such as mitosis and axonal transport. To determine whether previous photobleaching studies reported the behavior of axonal MTs properly and whether the MT behavior in mouse dorsal root ganglion (DRG) axon can be generalized to other quite different nervous systems, we performed photoactivation experiments on both mouse and *Xenopus* neurons in culture. When mouse sensory neurons were microinjected with caged fluorescein-labeled tubulin and then photoactivated, no movement of fluorescent MTs was observed. In contrast, forward movement of the photoactivated zone was frequently seen in rapidly growing axons of frog embryonal neurons. To see whether the mechanism of nerve growth might differ between two types of neurons, we analyzed the movement of the axon surface by monitoring the position of polystyrene beads adhering to the neurites. The results revealed anterograde movement of the beads on *Xenopus* neurons, but no such movement was observed on the mouse neurons. We conclude that the mode of transport of cytoskeletal polymers and some components of the axon surface differ between two neuron types, and MTs are stationary within the axon of mammalian neurons where the movement of the axon surface markers does not occur.

Materials and Methods

Preparation and Characterization of Caged Fluorescein-labeled Tubulin

Phosphocellulose-purified hog brain tubulin was labeled with bis-caged carboxyfluorescein-*N*-hydroxy-sulfosuccinimide ester (Biscaged-Fluorescein Sulfo OSu; Dojindo Laboratories, Kumamoto, Japan) according to the method of Mitchison (34). 5(6)carboxy-tetramethylrhodamine labeling of tubulin and BSA was described previously (43, 44). Caged fluorescein-labeled tubulin was activated as a drop under illumination of an UV hand lamp (365 nm for 5 min) and then examined by SDS-PAGE.

Observation of Caged Fluorescein-labeled MTs In Vitro

Caged fluorescein-labeled tubulin at 70 μM was polymerized in K-Pipes buffer (80-mM K-Pipes, 1 mM $MgCl_2$, 1 mM EGTA, pH 6.8) plus 4 mM $MgCl_2$, 30% glycerol, and 1 mM GTP at 37°C for 30 min. MTs were diluted in K-Pipes buffer plus 30% glycerol and 10 μM Taxol and examined under a fluorescent microscope (Axiophot; Carl Zeiss, Inc., Oberkochen, Germany) equipped with a silicon-intensifier target camera (SIT). For photoactivation, the full microscope field was exposed to 365-nm light using a Hoechst filter set and a mercury arc lamp for 3 s and then observed in the fluorescein channel.

Mammalian Cell Culture and Microinjection

Culture and microinjection of mouse DRG neurons were done as previously described (44). Cells were injected 5–10 h after plating and further incubated for 8–12 h. To identify injected neurons, cells were co-injected with caged fluorescein-labeled tubulin (50–100 μM) and rhodamine-BSA (0.5 mg/ml). BSC1 cells were grown in MEM (Gibco Laboratories, Grand Island, NY) containing 15 mM Hepes, pH 7.4, and 5% FCS. PtK2 cells were a generous gift from Dr. K. Izutsu (Mie University, Mie, Japan) and were grown in MEM supplemented with nonessential amino acids (Gibco Laboratories), 15 mM Hepes, pH 7.4, and 10% FCS. Cells were injected at interphase or at prophase and further incubated for 2 h for observation of the interphase MT network and for 10–30 min for observation of the mitotic spindle.

Microinjection of Caged Fluorescein-labeled Tubulin into Xenopus Embryos

Egg laying, in vitro fertilization, and dejelling were done as previously described (38). Two-cell embryos were microinjected in the animal pole of one blastomere with 30 nl of caged fluorescein-labeled tubulin (45 μM) (16). The eggs were allowed to develop to stages 22–25 and were then used for the isolation of neural tubes.

Culture of Xenopus Embryonal Neurons

Xenopus embryonal neurons were cultured according to the method of Kidokoro et al. (23). Briefly, the dorsal portion of embryos was isolated and incubated for 10–20 min in a collagenase solution (1 mg/ml type 4 collagenase, 67 mM NaCl, 0.5 mM $CaCl_2$, 1.6 mM KCl, 8 mM Na-Hepes, pH 7.4.). Spinal cords were isolated with a pair of fine needles and then incubated in a Trypsin solution (0.05% Trypsin, 0.53 mM EDTA, 67 mM NaCl, 1.6 mM KCl, 8 mM Na-Hepes, pH 7.4) for 5–10 min. Spinal cords were gently pipetted into culture chambers that were pretreated with laminin and filled with a medium containing 60% MEM, 15 mM Na-Hepes, pH 7.4, and 5% dialyzed horse serum. The cells were dissociated by repeated passage through a micropipette and maintained at 20°C.

Optical System for Photoactivation and Low Light Level Video Microscopy

The photoactivation apparatus was assembled according to the method of Mitchison (34) with slight modifications. A 365-nm beam generated by a mercury arc lamp and a band pass filter was introduced into the light path of an inverted microscope (Axiovert; Carl Zeiss, Inc.) via a dichroic mirror (390-nm-long pass) positioned between the original mirror box and the field diaphragm. Using a handmade slit, original dichroic mirror (390-nm long pass) and a neofluor 100×, 1.3 NA objective lens, it was possible to produce a microbeam with a width at half-intensity of 2.9 μm.

100-W halogen lamps were used for trans-illumination and for epi-illumination at high magnification. For the search of injected cells at low magnification, a 100-W mercury lamp in combination with neutral density filters was used as a light source of epi-illumination. To avoid excess illumination, the 365-nm microbeam and epi-illumination were controlled by electronic shutters. Differential interference contrast (DIC) images were projected via a lateral light exit to a television camera equipped with an analogue contrast enhancement circuit (model C2400-07; Hamamatsu Photonics, Hamamatsu, Japan) the video frames were then mottle subtracted and averaged using an image processor (ARGUS-100; Hamamatsu Photonics). Fluorescent images were collected using an image intensifier coupled with a charge-coupled device (CCD) camera (ICCD camera, model C2400-87; Hamamatsu Photonics) or a cooled CCD camera (model C3640; Hamamatsu Photonics). Images were stored on tape using an SP.U-matic video cassette recorder (model VO-9600; SONY, Tokyo, Japan) or on an optical disk recorder (model RS-92000, RICOH, Tokyo, Japan).

Photoactivation and Video Microscopy

The microinjected cells were precisely positioned with the aid of a mark on a filter placed on the back focal plane of the objective lens. Culture chambers containing injected cells were placed on a thermostatted stage and maintained at 35°C for mammalian cells and at 20–25°C for *Xenopus* neurons. The 365-nm microbeam was applied for 0.25–0.5 s and further illumination did not increase fluorescence intensity. After photoactivation, fluorescence images were collected sequentially using the ICCD or the cooled CCD camera. For the ICCD camera, cells were illuminated for 0.75–1.0 s and 20–30 video frames were summed, averaged, background subtracted, and stored. The cooled CCD camera contained a 1,024 × 1,024 pixel chip and was electronically cooled to −30°C. By inserting an electronic shutter interfaced to the image processor, exposure time was controlled to 0.5–1.0 s. Images were digitized to 16-bit depth and dark current noise was corrected digitally.

Preparation and Application of Membrane Markers

Fluorescent polystyrene microspheres (Polysciences Inc, Warrington, PA)

1.0 μm in diameter were coated with polyethyleneimine (Polysciences Inc.) according to the method of Zheng et al. (55) or coated with laminin (Gibco Laboratories) by incubating 0.8% (wt/vol) of beads in 50 μg/ml of laminin for 1 h. 0.8% (wt/vol) suspension of coated beads (10 μl) was added to the stage medium (2–3 ml). By adjusting the focus of DIC images, we could determine whether fluorescent beads were on the cell surface or inside the cytoplasm. Generally, internalization of large fluorescent beads into the neuronal cytoplasm was rare.

Data Analysis

The time of a complete turnover of MTs was the last time point at which the photoactivated regions were still discernible from adjacent regions.

For all measurements of translocation rates, drift of the culture substrate was checked by monitoring the position of debris adhering to the substrate. The translocation rate of the photoactivated regions were determined as follows: (*a*) When the neurites did not change their direction and the cell bodies did not move on DIC images, the distance between the centers of the photoactivated regions in the first and last frames were calculated on the CCD image processor. (*b*) When the neurites changed their direction or the cell bodies moved, the positions of photoactivated zones were marked on prints of DIC images by superposition of fluorescent images at the nearest time points. The distance from the base of the neurite to the photoactivated zone were measured and the increase of the distance during the observation period was determined.

To measure the length of a photoactivated region, pixels, which were more than half of the intensity of the maximum value, were extracted and the width of this pixel cluster along the neurite was determined.

The translocation rates of polystyrene beads were determined by plotting the position of the beads on transparent sheets directly from a monitor and summing the distance of the beads' position between two successive video images. The summation of translocation distance were then divided by the time between the first and last frames. Only straight neurites with no lateral movement during recording were used for translocation rate measurements of polystyrene beads.

The generation of intensity profiles of digitized images on an image processor was described previously (44).

Other Methods

Biotin-labeled tubulin was prepared as described previously (24). The methods of immunoelectron microscopy of injected neurons were previously described (42, 44).

Results

Characterization of Caged Fluorescein-Conjugated Tubulin and Photoactivation Procedure

Tubulin molecules were conjugated with bis-caged carboxyfluorescein. Fig. 1 *a* shows SDS-PAGE of the preparation of bis-caged carboxyfluorescein-labeled tubulin. Labeled tubulin preparations were nonfluorescent before UV illumination (lanes *2* and *4*) and became fluorescent only after photoactivation (lanes *3* and *5*). When caged fluorescein-conjugated tubulin was polymerized in vitro and then activated, MTs became visible as long straight fluorescent filaments (Fig. 1, *b* and *c*). To confirm that caged fluorescein-labeled tubulin can be incorporated in vivo into the MT network and turn over normally, we microinjected this preparation into cultured cells and activated a narrow zone both in interphase and in mitosis by irradiation with a 365-nm microbeam. After activation of interphase cells, fluorescent MTs were observed and turned over with an approximate half time of 15–20 min (data not shown), in good agreement with previous estimations by different methods (47, 48, 49). To observe behavior of photoactivated MTs in mitosis, PtK2 cells were injected in prophase and were illuminated with a 365-nm microbeam during metaphase. Over 10 min, the bar of fluorescence across the spindle decreased in intensity and moved toward the spindle pole during observation (data not shown). This result is consistent with the report of Mitchison (34), supporting the fact that our preparation of labeled tubulin and the method of photoactivation did not interfere with the biological motile processes.

Photoactivated MTs Are Stationary in Growing Axons of Mouse Sensory Neurons

To examine the possible movement of tubulin during axon elongation, we microinjected caged fluorescein-labeled tubulin into cultured mouse DRG neurons. We chose adult mouse sensory neurons for the following reasons. First, adult mouse sensory neurons have large cell bodies (25–60 μm in diameter) and this facilitates the microinjection procedure and the introduction of large amounts of labeled tubulin. Second, we can obtain the homogeneous population of neurons that begin to extend neurites within a relatively short period of 5–10 h after plating. Third, the growth rate of the adult DRG neurons on the laminin-coated substrate is maximal among variety of the combinations of mammalian neuron types (embryonal cerebral, cerebellar, spinal cord, and sensory neurons) and of culture substrates (poly-lysine, collagen, and fibronectin) (our own unpublished results). Furthermore, the growth rate (10–80 μm/h) of adult mouse sensory neurons is faster than or equal to several well-established culture systems of primary neurons (1, 2, 5, 13).

Neuron cell bodies were injected 5–10 h after plating, at a time when the DRG neurons had not yet extended neurites or had sprouted only short processes (<100 μm). During the successive period of 10–24 h after plating, the neurite elongation rate reached the maximal value for this neuron type. Therefore, photoactivation experiments were performed 8–12 h after injection (namely, 13–22 h after plating). To confirm that injected tubulin molecules are incorporated into all MTs in the axon, we microinjected biotin tubulin into DRG neurons 10 h after plating, permeabilized and fixed the injected cells 8 h after injection, and then processed them for immunoelectron microscopy with an antibiotin antibody. As shown in Fig. 2, almost all MTs along the length of nerve processes (entire length of 10 processes of five different injected neurons were examined) were decorated with gold particles, indicating that the injected tubulin molecules completely shuffled with endogenous tubulin pool at the period of photoactivation and successive observation.

The processes of the DRG neurons generally had a complex morphology with many ramifications, a common feature of this neuron type when plated on laminin-coated surfaces (32). During neurite elongation, the distal segments of neurites contributed to the increase in neurite length and the proximal segments did not change their position and shape. This property is clearly shown in Fig. 3, *g* and *h* (see also Fig. 13, *e–g*). After transformation of the growth cone into newly made neurite, the position of branch points (*arrowheads* in Fig. 3, *g* and *h*, and see Fig. 13, *d–g*) and the lengths of neurites between branch points did not change. Furthermore, the diameter of proximal neurites did not decrease significantly (Fig. 3, and see Fig. 13). This growth pattern makes the estimation of the net increase of axonal structure easier, since the effect of neurite straightening and thinning can be neglected.

For fluorescence activation, we chose neurons with processes longer than 200 μm and with active growth cones.

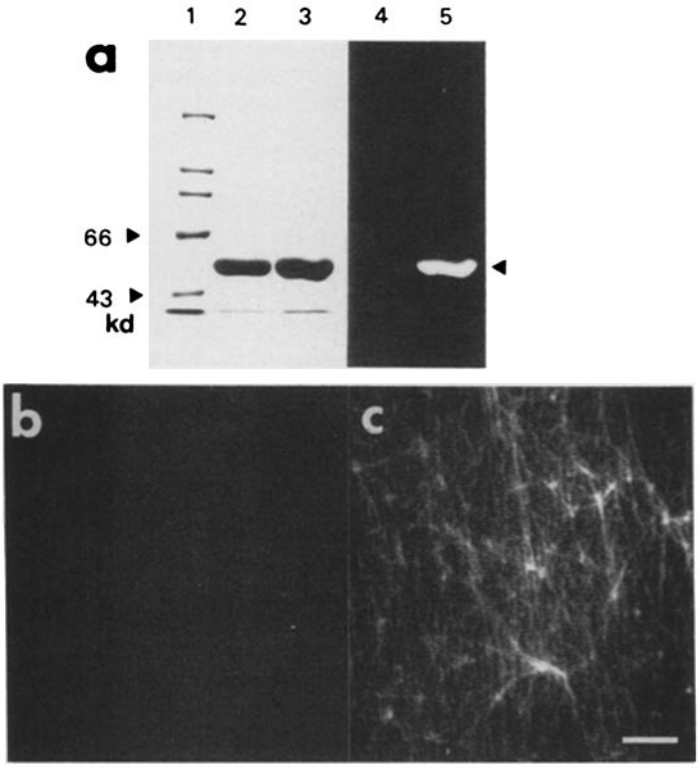

Figure 1. Characterization of caged fluorescein-labeled tubulin. (*a*) SDS-polyacrylamide gel analysis of the preparation of bis-caged carboxyfluorescein-labeled tubulin. Labeled tubulin preparations before (lanes *2* and *4*) and after activation (lanes *3* and *5*) were analyzed by dye staining (lanes *2* and *3*) and by UV illumination (lanes *4* and *5*). Labeled tubulin molecules became fluorescent only after photoactivation (*arrowhead* in lane *5*). (Lane *1*) Molecular mass standards. (*b* and *c*) Fluorescent images of caged fluorescein-labeled tubulin assembled in vitro. Before activation, no fluorescent fibers can be detected (*b*). After activation (for 3 s with 365-nm light), many straight filaments can be observed (*c*). Bar, 10 μm.

A small zone of the neurite was illuminated with a 365-nm microbeam for 0.5 s and the movement of fluorescent MTs was monitored. Fig. 3 shows an example of a photoactivation experiment. Two photoactivated zones were placed on the proximal part of an axon and fluorescence images were taken sequentially to analyze both the position of the fluorescent zone and the axonal growth. No significant movement of the photoactivated zones was observed throughout this experimental run. Fig. 3 *i* shows intensity profiles of the photoactivated region at 1 and 75 min after microbeam irradiation. Although the shapes of the two peaks changed with time, the centers of the two peaks did not move forward. During this observation, the neurites elongated rapidly and the total increase in length of the distal branches shown in Fig. 3 *h* was 88 μm. Behavior of fluorescent MTs was independent of the position of the photoactivation. Figs. 4 and 5 show behavior of MTs photoactivated in the middle and distal parts of neurites. As before, in both cases no translocation of MTs was observed, while these neurites elongated by 43 and 17 μm during the periods of observations (Figs. 4 and 5, respectively).

We analyzed 23 photoactivated zones in 20 growing neurons. The 23 runs can be divided into the following categories: (*a*) Proximal activation. Fluorescent marks were placed within 50 μm from the cell bodies (11 of 23 examples); (*b*) Middle activation. Fluorescent marks were placed >50 μm away from cell bodies and >50 μm away from the growth cones (7 or 23 examples; and (*c*) Distal activation. Fluorescent marks were placed within 50 μm from growth cones (5 of 23 examples). Regardless of the position of photoactiva-

Figure 2. Immunoelectron microscopy of a neurite of the DRG neuron permeabilized and fixed 18 h after plating and 8 h after injection of biotin-tubulin, and then reacted with an antibiotin antibody and a colloidal gold-labeled secondary antibody. All MTs are heavily decorated with gold particles. Bar, 200 nm.

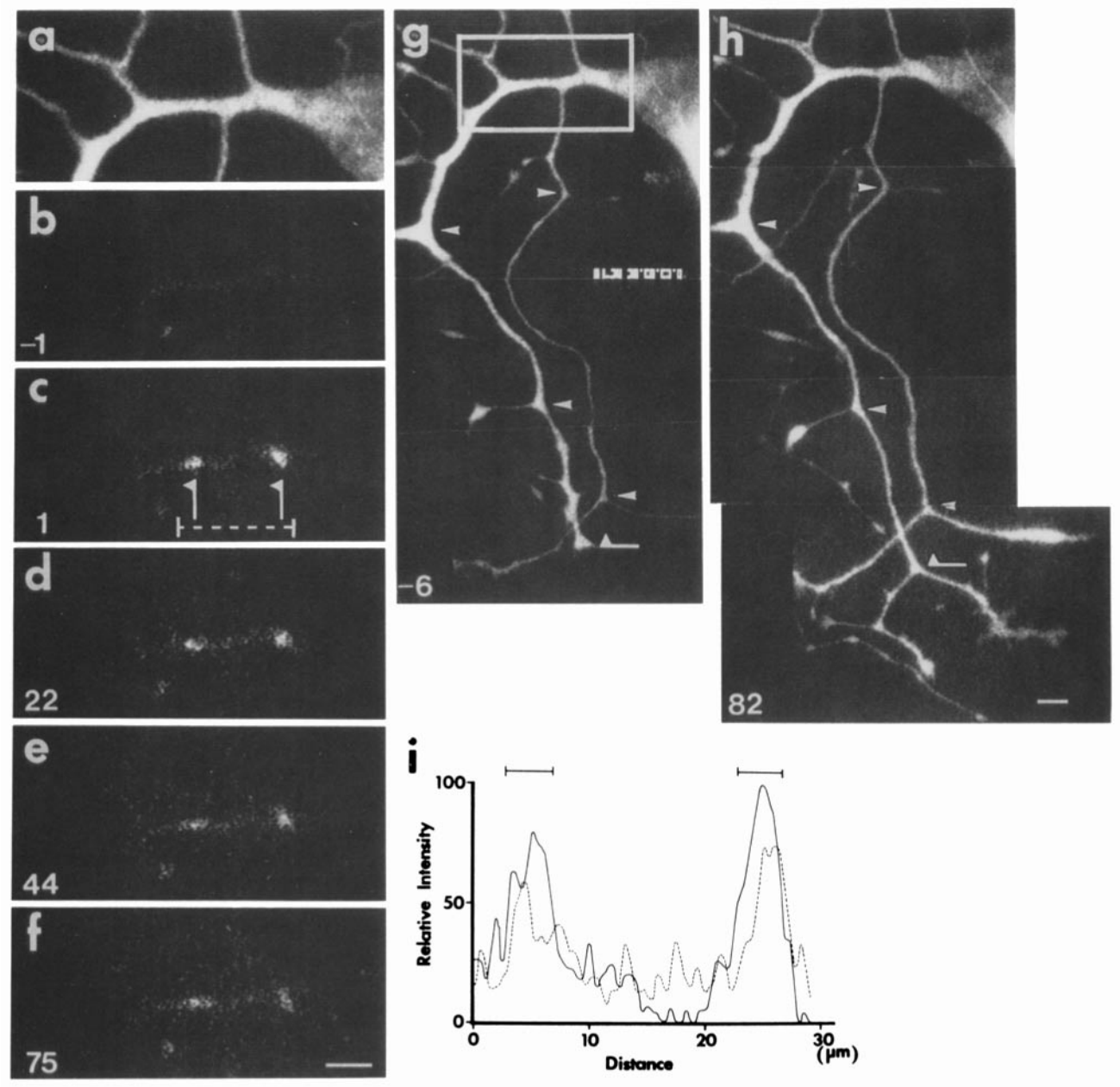

Figure 3. Photoactivation of MTs in the proximal part of the growing axon of a mouse sensory neuron. Cells were injected with caged fluorescein-labeled tubulin and rhodamine-labeled BSA simultaneously. Before activation, the whole structure of the growing axon was recorded by illumination with a green light. The rectangle in *g* indicates the field presented in *a–f*. On the proximal part of the axon visualized by rhodamine-BSA (*a*), two photoactivated zones were generated (*arrows* in *c*). The photoactivated zones remained in the same position for >1 h. After the experimental run, a fluorescent image with a rhodamine filter set was again obtained (*h*). Arrows in (*g* and *h*) show the position of the axon tip before photoactivation and arrowheads in (*g* and *h*) show the branching points that were stationary throughout the experiment. During this experimental run, the axon elongated significantly, with the combined increase in length being 88 μm. Intensity profiles of photoactivated regions (*i*) were created from digital images (*c* and *f*). Solid line shows the profile just after the photoactivation and dashed lines correspond to that 75 min after photoactivation. Two bars (*i*) indicate the position of photoactivated regions. The area presented in *i* is shown as dotted lines in *c*. Elapsed time (min) after photoactivation is shown in the lower left-hand corner of each panel. Bars, 10 μm.

tion, we observed no translocation of fluorescent MTs in mouse DRG neurons.

Turnover of photoactivated zones in the axon was much slower than that in fibroblasts, and the mean time required for a complete turnover of fluorescence was 57.4 ± 6.9 min (n = 23). Since soluble tubulin subunits would diffuse from the site of activation within 1 min (27, 43), the observed slow decrease of fluorescence is likely to represent the turnover of assembled tubulin polymers. This turnover rate is in good agreement with previous photobleaching experiments on fluorescent MTs in growing axons (30, 31, 43).

Photoactivated MTs Translocate in Growing Axons of Xenopus Embryonal Neurons

To see whether the behavior of MTs differs between the two

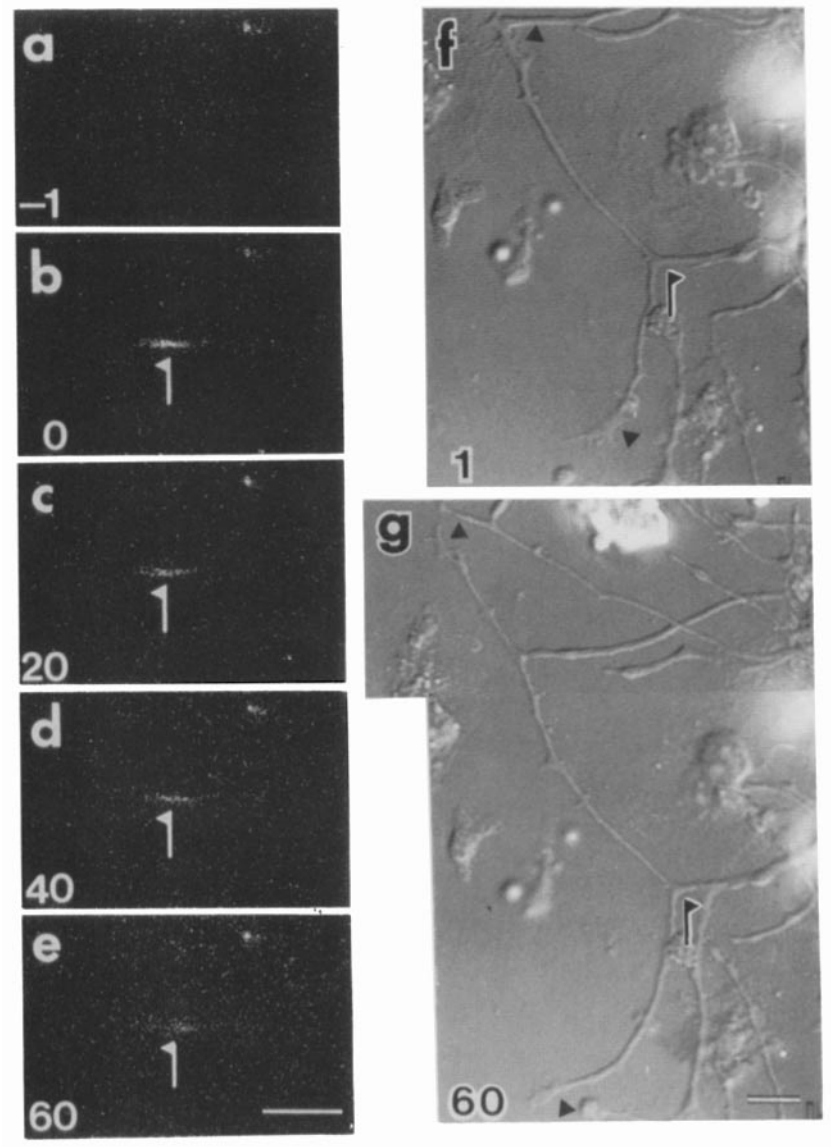

Figure 4. Photoactivation run on the middle part of the growing axon of a mouse DRG neuron. (*a–e*) Fluorescence images of the axon indicating that the fluorescent zone generated by irradiation of 365-nm light (*arrows*) is stationary. (*f* and *g*) DIC images of the photoactivated neurite. Arrows indicate the position where the photoactivation pulse was applied. During this experimental run, the growth cones (*arrowheads* in *f* and *g*) advanced rapidly and the combined length of the newly formed neurites was 43 μm. Elapsed time (min) after photoactivation is shown in the lower left-hand corner of each panel. Bars, 10 μm.

neuronal types, we characterized the mode of axonal growth and MT behavior in frog neurons. Neurons dissociated from *Xenopus* embryo spinal cords attached to the culture surface and extended neurites most effectively when the culture surface was coated with pure laminin. *Xenopus* neurons were less adhesive to bare glass surface and collagen-coated coverslips. On the laminin-coated surfaces, *Xenopus* neurons projected long processes tipped with highly motile growth cones. Neurite growth was very rapid (60–250 μm/h) in comparison with cultured mammalian or avian neurons (10–80 μm/h). We did not attempt to analyze the process outgrowth from the explants of the neural tubes, since precise determination of the position of cell bodies and proximal neurites is impossible in explants.

We recorded neurite growth of 22 *Xenopus* neurons using video-enhanced DIC microscopy. Observations were done intermittently at intervals of 5 min and the observation periods ranged from 30 min to 6 h. Fig. 6 shows a typical growth pattern of *Xenopus* neurons on laminin-coated surfaces. We chose this example since the observed cell was not in any way atypical and was followed for a relatively long period. The cell initially had a single neurite tipped with a large growth cone (surrounded by *arrowheads* in Fig. 6, *a–d*, *f*, and *g*). At 10 min, a branch (*arrow* in Fig. 6 *b*) was generated by the bifurcation of the growth cone. After the branch was formed, the segment proximal to the branch point shortened rapidly and was lost completely at 21 min (Fig. 6 *c*). During the next 65 min, the two branches from the common trunk were transformed to two neurites extending directly from opposite sides of the cell body (Fig. 6, *c–e*). After the establishment of two neurites extending in opposite directions, the sprouting of a third neurite from the cell body was seldom observed. During the period between 86 and 164 min, the two growth cones were relatively quiescent but the translocation of the cell body (*asterisks*) toward the right growth cone resulted in the shortening of the right neurite (*arrow* in Fig. 6 *f*). From 164 to 275 min, rapid growth of the right neurite (*arrows* in Fig. 6, *f–h*) started. The growth cone was large and active (surrounded by *arrowheads* in Fig. 6, *f* and *g*) and went out from the field presented in Fig. 6 *h*. Finally, a bipolar neuron was established (Fig. 6 *i*). Such bipolar neurons are common at later stages of culture. In the

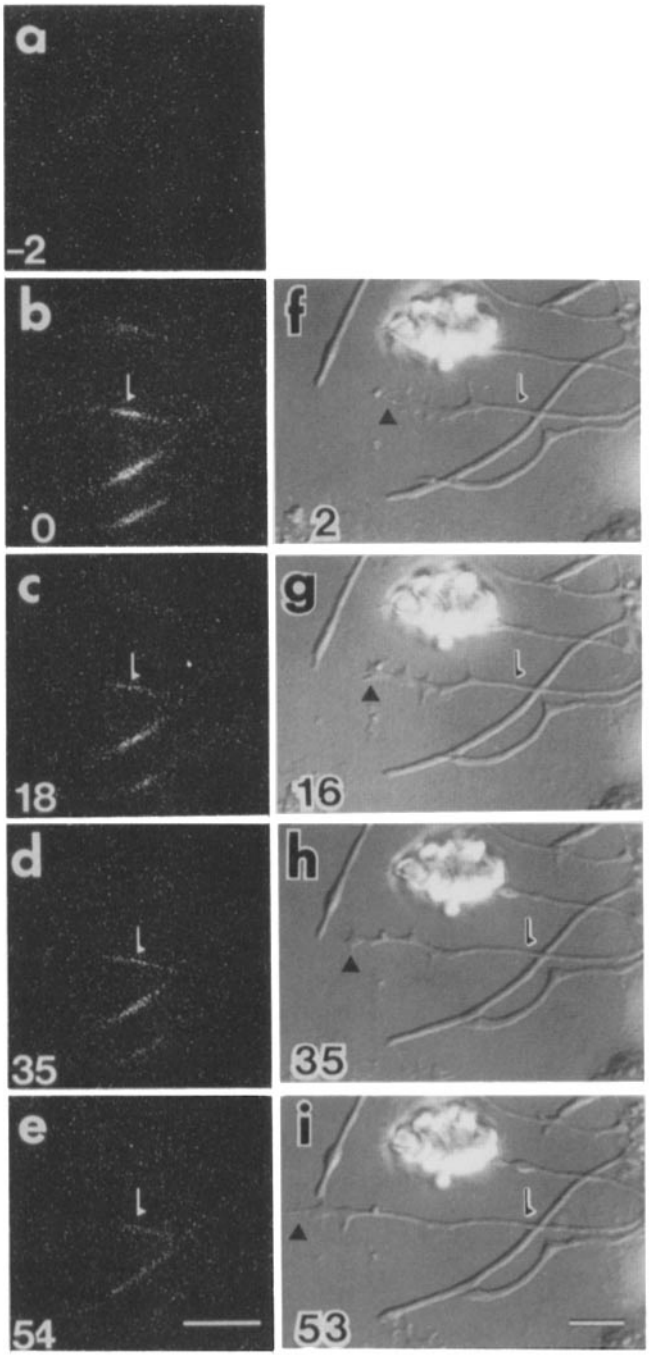

Figure 5. Photoactivation run on the distal part of the growing axon of a mouse DRG neuron. (*a–e*) Fluorescence images of the photoactivated axons. The photoactivated regions (*arrows*) remained in the same position along the axon. (*f–i*) DIC images of the photoactivated neurites. During this experimental run, one of the photoactivated neurites elongated by 17 μm (*arrowheads*). The arrows indicate the position of the photoactivated region on this rapidly growing neurite. Elapsed time (min) after photoactivation is shown in the lower left-hand corner of each panel. Bars, 10 μm.

process of rapid growth of neurites, progressive thinning of neurites was generally observed. For example, in the left branch, from 21 to 86 min (Fig. 6, *c–e*), and in the right neurite, from 164 to 275 min (Fig. 6, *f–i*), caliber decreased. This progressive decrease in the diameter is more clearly observed at higher magnification (Fig. 6, *j–l*). In summary, the shafts of *Xenopus* neurons continued to change their shape and decreased their diameter during process elongation. As shown in Fig. 6, branch points of neurites, formed by the bifurcation of the growth cone, did not retain their shape for a long period because shortening of the proximal trunk, or collapse and withdrawal of one of the two branches frequently occurred. As a result, the number of branching points per process was usually zero or one and never exceeded five during the first day in culture.

We first injected rhodamine-conjugated tubulin into *Xenopus* embryos at the two-cell stage and allowed them to develop to stages 22–25 before isolating neurons. The growing neurites of cells isolated from the injected embryos contained fluorescent MTs (Fig. 7), indicating that injected derivatized tubulin molecules are retained in cultured neurons and function normally. We next introduced caged fluorescein-labeled tubulin into *Xenopus* embryos and neural tubes were isolated and cultured.

Photoactivation experiments were performed 2–10 h after plating, a time point at which the neurite elongation rate was maximal. Since cell bodies of *Xenopus* neurons tended to be unattached to the substrate and were often pulled across the dish, we chose neurons with short neurites (<100 μm) for photoactivation and the position of cell bodies was monitored using DIC images without moving the microscope stage. When a narrow zone of rapidly extending neurites was illuminated with a 365-nm microbeam, anterograde movement of the photoactivated zone was frequently observed. Fig. 8 shows an example of the photoactivation experiments. In this case, the cell body was pulled across the culture surface and we calculated the distance between the base of the neurite and the photoactivated zone by superposition of fluorescent and DIC images. The distance changed from 22 to 32 μm during the 16-min observation, indicating forward movement of MTs relative to the cell body. Of 24 photoactivation experiments using rapidly growing neurites, 15 photoactivated zones showed forward movements relative to the cell body and the others did not. The translocation rate varied significantly from experiment to experiment and ranged from 12 to 175 μm/h with a mean and standard error of 58 ± 11 μm/h (n = 15).

The relation between the translocation rate of the photoactivated zone and the rate of axonal growth was complex. In some cases, movement of the photoactivated zones was rapid and seemed to keep up with the growth cone advance (Fig. 8). In other cases, however, the photoactivated zones moved much slower than the growth cones, resulting in a formation of new fiber structure distal to the photoactivated region (Fig. 9).

Turnover of photoactivated MTs was much faster than that in the axons of mouse sensory neurons, and we could follow the position of fluorescent zones only up to 20 min after photoactivation of rapidly growing axons of *Xenopus* neurons. Since exchange half time of free tubulin molecules would be <1 min within the axon (43), it is less likely that photoactivated tubulin molecules were largely in nonassembled state.

To see whether the photoactivated zones become broader during translocation, the widths of the fluorescent regions were plotted against the translocation distances. As shown in Fig. 10, the photoactivated MT segments moved out from their initial position without significant spreading. These results suggest that fluorescent MTs are not likely to be slid-

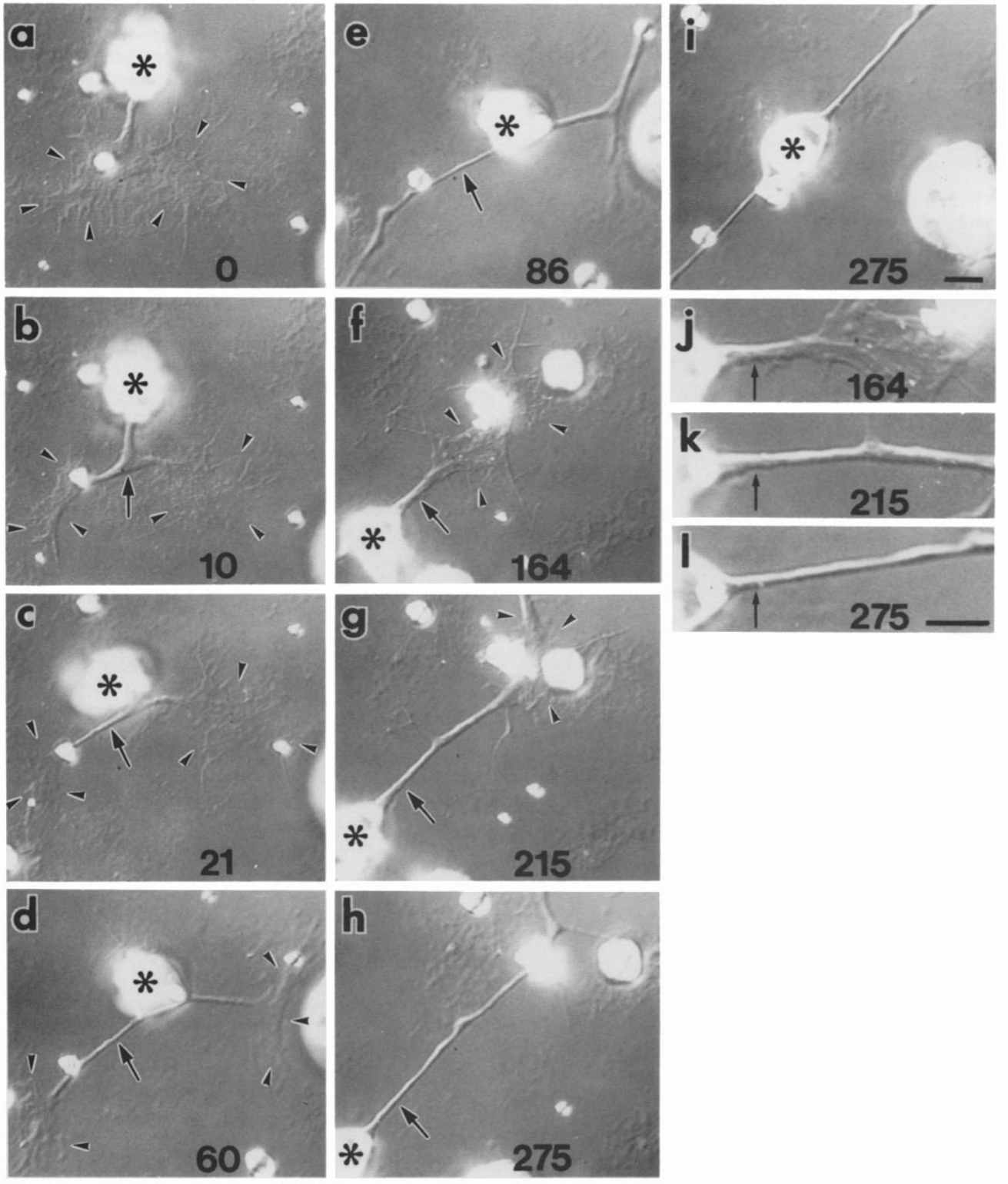

Figure 6. DIC images of a growing *Xenopus* neuron. The process of initial sprouting of a growth cone (surrounded by *arrowheads* in *a–d*, *f*, and *g*) and subsequent development of the bipolar structure (*i*) were presented. (*a–i*) DIC images recorded intermittently from 0 to 275 min. The cell body (*asterisks*) was loosely attached to the substrate and changed its position throughout this experimental run. By 10 min, the bifurcation of the growth cone did occur and a branch point was formed (*arrow* in *b*). From 10 to 86 min, the left branch elongated rapidly (*arrows* in *c–e*) and the proximal trunk shortened simultaneously. As a result, the bipolar form of the neuron began to be established. From 164 to 275 min, rapid growth of the right neurite occurred and the right growth cone (surrounded by *arrowheads* in *f* and *g*) went out from the field presented in (*h*). In (*i*), the typical arrangement of the neurites of *Xenopus* neurons, namely two straight thin neurites extending toward the opposite directions, can be observed. (*j–l*) Higher magnification view of the proximal part of the right neurite. Progressive thinning of the neurite can be observed (*arrows*). Times in minutes relative to the first frame in *a* are shown in the lower part of each panel. Bar, 10 μm.

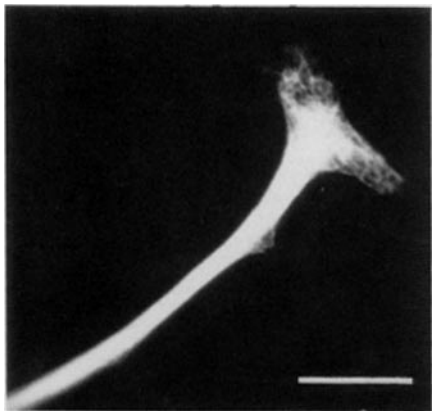

Figure 7. Fluorescent image of the growth cone and the neurite of a neuron isolated from a *Xenopus* embryo injected with rhodamine-labeled tubulin. Fluorescent MTs can be observed in the growth cone. Bar, 5 μm.

ing as individual filaments, but rather to be translocating en bloc.

Axon Surface Movements of Two Neuron Types Are Different

Since the photoactivation experiments raised the possibility that the mechanism of nerve growth might differ between two types of neurons, it would be intriguing to analyze the movement of other axonal components during process extension. An indication of another major difference between the two types of neurites emerged from the DIC images. For the *Xenopus* axons, we frequently observed anterograde movements of cell debris adhering to the neurites. The arrowheads in Fig. 8, *h–l* and Fig. 9, *f–h* indicate the positions of cell debris adhering to the neurite shaft, and anterograde movement of these particles is observed. The particles attached near the photoactivated zone tended to move at a similar velocity with the fluorescent MTs (Fig. 8). These observations suggest that some components of the *Xenopus* axon surface move toward the axon tip. To further characterize the behavior of the axon surface, we added fluorescent beads coated with polyethyleneimine or laminin to culture medium and monitored the positions of microspheres adhering to the neurites. Fig. 11 shows the growing axon of a *Xenopus* neuron decorated with fluorescent polystyrene beads. Forward movements of two microspheres can be observed (*arrows*) and the position of the beads was confirmed by fluorescent images (Fig. 11, *b* and *g*). To quantitate the translocation rate of the beads shown in Fig. 11, the distance of two microspheres from the initial position of the more proximal one was plotted against time. As shown in Fig. 12, the translocation rates of the two beads were not identical and the distance between the two moving beads increased by ~60% (from 15 to 24 μm). Since the axonal diameter did not reduce significantly during the course of the experiment, it is unlikely that the observed movement of the fluorescent beads can be because of mere elastic stretching of the axon. From the measurements of 13 moving beads on seven growing axons (polyethyleneimine-coated beads: 7 of 13 examples; laminin-coated beads: 6 of 13 examples), the translocation rate was estimated to be 89.4 ± 9.3 μm/h (n = 13).

In striking contrast, when growing neurites of mouse DRG neurons were marked with fluorescent beads, no net distal motion of the beads was observed. For example, in Fig. 13, two microspheres (*arrows*) initially on the dorsal surface of a large growth cone remained in the same position during neurite elongation, that resulted in the formation of 50 μm of new neurites distal to the microspheres. We analyzed the position of 10 particles over eight rapidly advancing growth cones or neurites and no overall distal motion from the cell body was observed. This result is consistent with previous reports using mammalian neurons in culture (4, 14, 45, 55), suggesting that the axon surface is stationary during the neurite growth of mammalian neurons.

Discussion

Most Microtubules Are Stationary in Mouse Sensory Neurons, but Move in Block within Xenopus Embryonal Neurons

We report here striking differences in the behavior of photoactivated MTs in two neuron types. First, using photoactivation of caged fluorescein-labeled tubulin in mouse sensory neurons, no movement of photoactivated tubulin can be detected. This finding supports previous experimental efforts reported for mammalian and avian axons. Namely, several preceding efforts using photobleaching of fluorescently labeled tubulin injected into mammalian and avian neurons have revealed that the bulk of MTs is stationary in the axon (30, 31, 43). Our results thus confirm and extend the photobleaching results.

Second, using a similar experimental approach, photoactivated tubulin is translocated anterogradely in block during rapid neurite extension of *Xenopus* neurons. During the last revision process of this paper, the paper of Reinsch et al. (46) has appeared and they have also found rapid anterograde movement of essentially all axonal tubulin in *Xenopus* embryonal neurons. Although the report of Reinsch et al. (46) is generally consistent with our study, we will briefly discuss two major differences between the two studies on the same material. (*a*) Reinsch et al. (46) stated that in almost all experimental runs translocation of photoactivated zone was observed. In contrast, we observed translocation of photoactivated zone in only 60% of the runs. One possible explanation of this discrepancy is that our photoactivation technique is inadequate and interferes with the process of MT translocation. Otherwise, the observation of Reinsch et al. (46) might involve the case where the movement of cell bodies occurs (this phenomenon is mentioned in the result section) and overestimate the translocation frequency, since they mainly used explant cultures and the position of cell body is difficult to monitor in explants. (*b*) Reinsch et al. (46) stated that the loss of photoactivated fluorescence can be explained by the photobleaching during observation and the nonuniform illumination of the camera field. We observed a significant decrease (<40%) of fluorescence during 20 min of observation. Since we used a cooled CCD camera, which is linear with input light levels over the entire dynamic range, and we restricted the total exposure time to only 6 s, which has been shown to cause fluorescence loss of <10% (our own unpublished results), we think the decrease of fluorescence is not an experimental artifact. Despite these differences, two

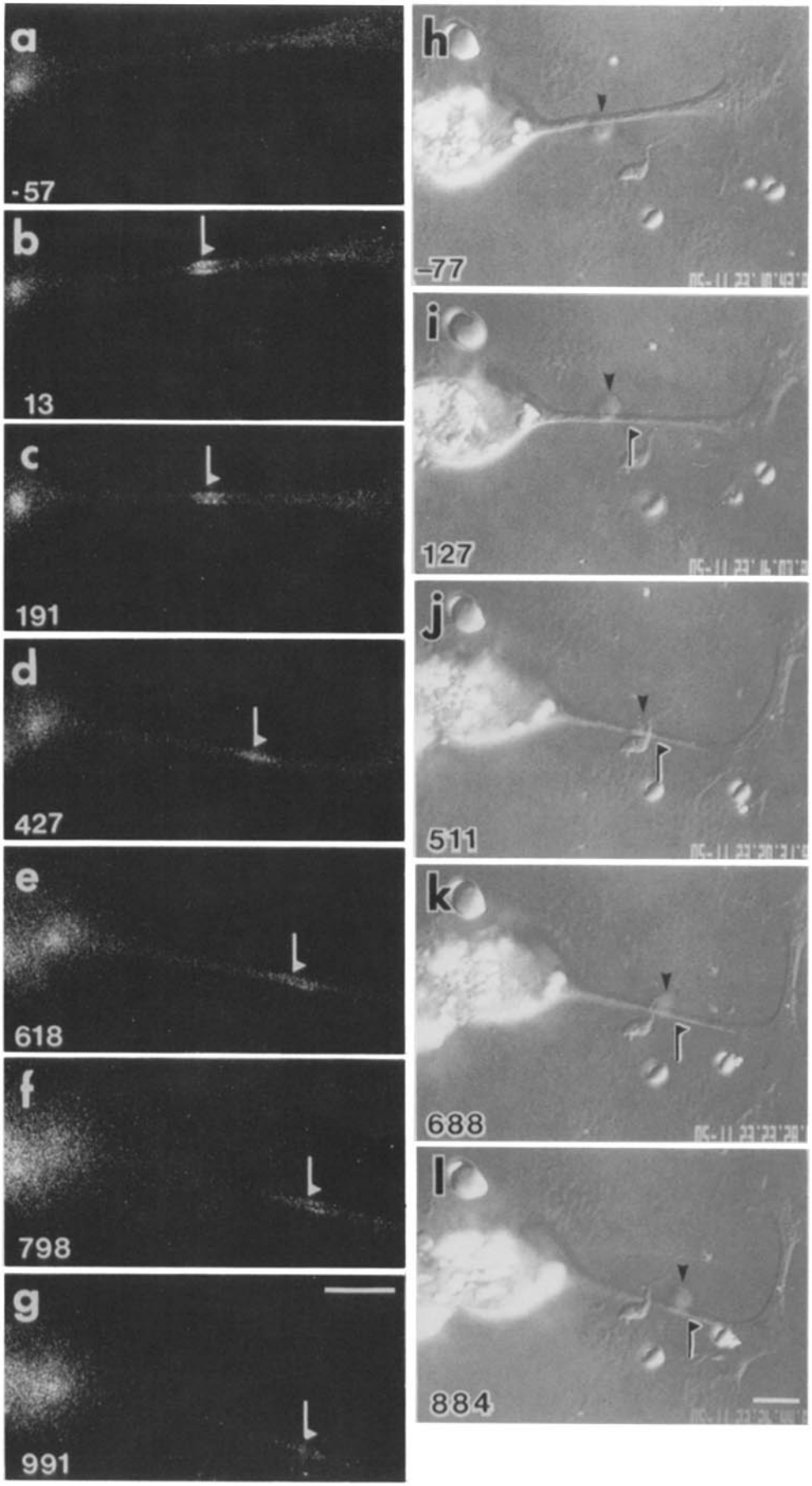

Figure 8. Photoactivation of MTs in the growing neurite of a *Xenopus* embryonal neuron. (*a–g*) A photoactivation run in a growing *Xenopus* neuron. Forward movement of a photoactivated zone can be observed (*arrows* in *b–g*). (*h–l*) DIC images of the same neuron during the photoactivation run. The growth cone was highly active and the direction of the neurite shaft changed gradually as the growth cone moved laterally. The cell body also translocated forward during observation. Arrows in DIC images indicate the position of photoactivated zones determined by superposition of fluorescent images at the nearest time points. Anterograde movement of a piece of debris adhering to the neurite (*arrowheads* in DIC images) was also observed through this experimental run. Times in seconds relative to the photoactivation pulse are shown in the lower left-hand corner of each panel. Bars, 10 μm.

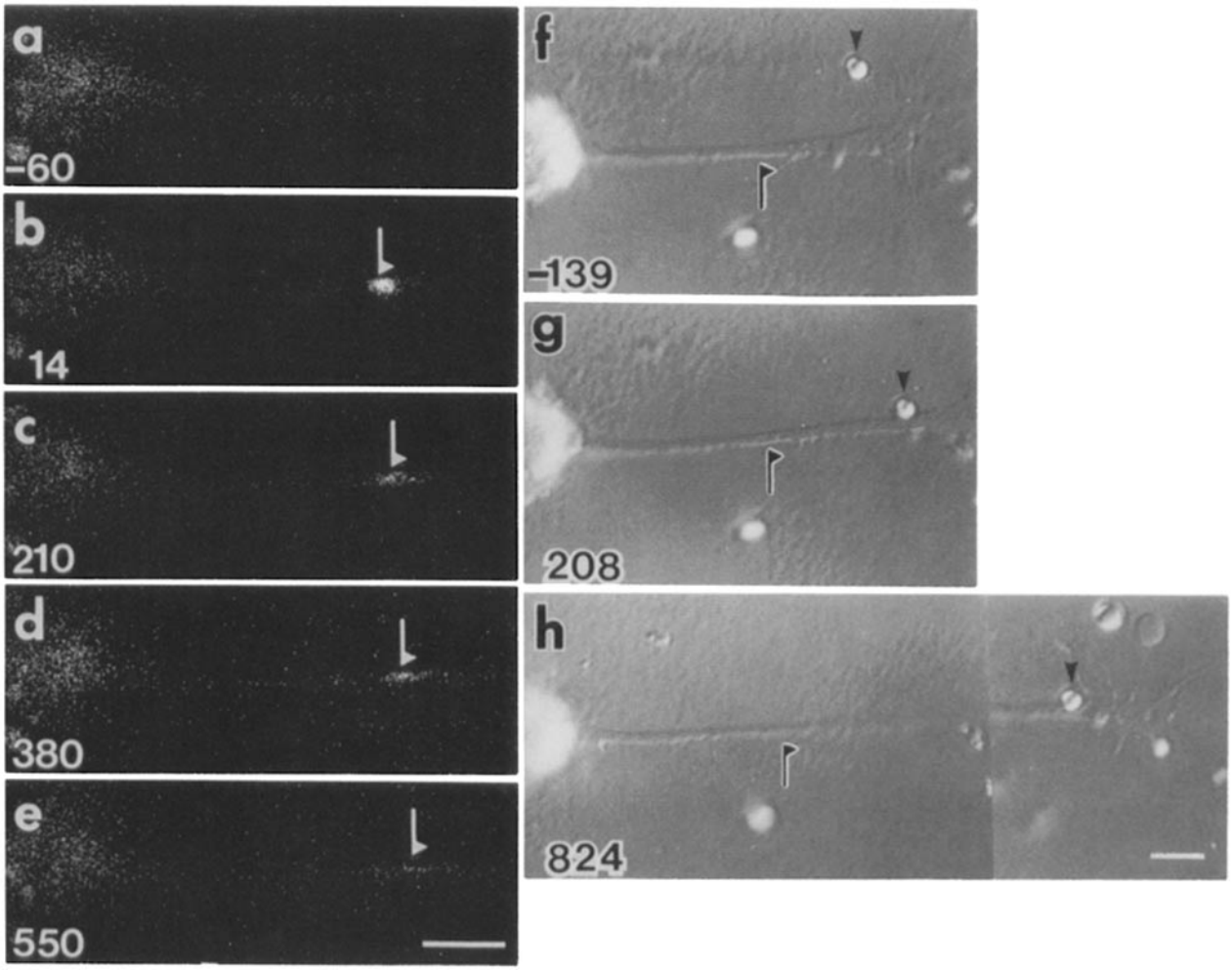

Figure 9. Photoactivation run in a growing neurite of a *Xenopus* neuron. (*a–e*) Fluorescent images of photoactivated MTs in a growing neurite. Forward movement of a photoactivated zone can be observed (*arrows*). (*f–h*) DIC images of the same neuron during photoactivation run. The photoactivated region is indicated by arrows. During the observation, the neurite was elongated by 43 μm. Arrowheads in DIC images indicate the position of a piece of debris, which was free from the substrate (*f*), and then adhered to the neurite (*g*). After attachment, the debris translocated forward (*g* and *h*) as the growth cone advanced. Elapsed time (sec) after photoactivation is shown in the lower left-hand corner of each panel. Bars, 10 μm.

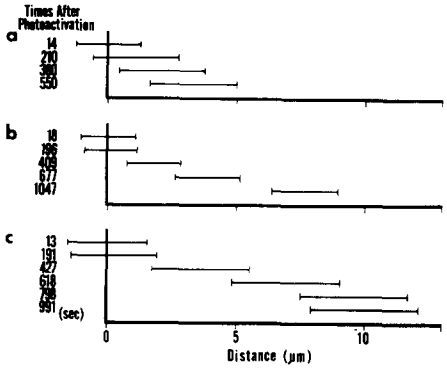

Figure 10. Length of photoactivated zones vs. translocation distance along the neurites. (*a–c*) shows independent photoactivation runs and *a* and *c* correspond to the cells shown in Fig. 9 and Fig. 8, respectively. Regardless of the translocation rate, photoactivated zones moved out from their initial position without significant spreading.

reports clearly revealed in block translocation of photoactivated tubulin molecules in *Xenopus* axons.

There are several potential technical explanations for the difference between mammalian and *Xenopus* neurites. First, the difference might arise if the modified tubulin somehow inhibited transport of MTs or tubulin oligomers into which it incorporated. In this instance, after photoactivation, a moving tubulin phase would not be observed. However, incorporation of caged fluorescein-labeled tubulin into interphase networks of MTs and mitotic spindles and successive photoactivation did not affect dynamics of MTs and motile processes such as chromosome movement and poleward MT flux. Microinjection of labeled tubulin into frog two-cell embryos did not perturb the normal development, suggesting that caged fluorescein-labeled tubulin function and turnover normally during development in situ. Furthermore, our immunoelectron microscopic observations of DRG neurons injected with biotin-tubulin indicated homogeneous incorporation of biotin-tubulin into all MTs in the neurites 8 h after

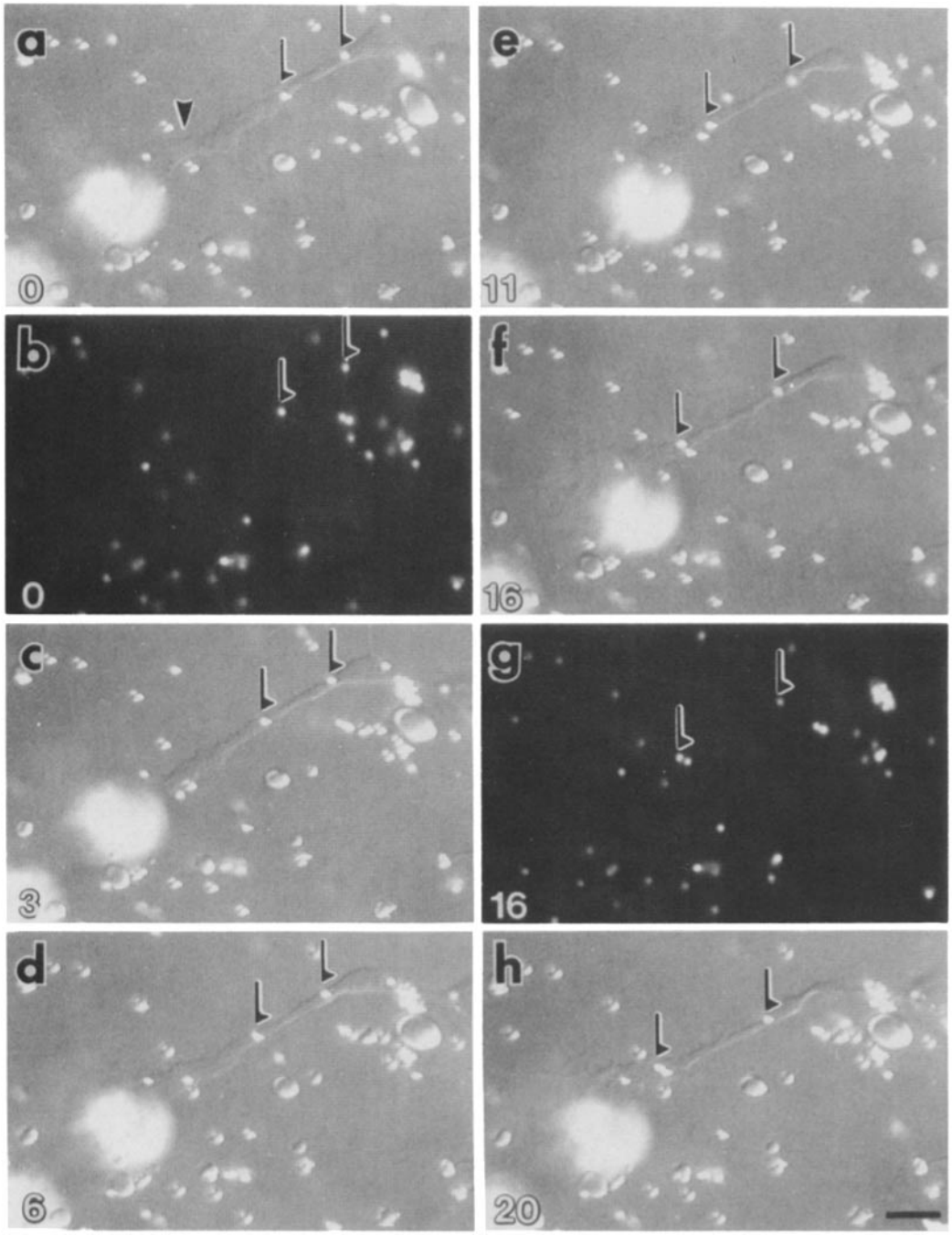

Figure 11. DIC images of a growing *Xenopus* neurite decorated with fluorescent polystyrene microspheres. Elapsed time (min) after recording of the first frame is shown in the lower left-hand corner of each panel. Forward movement of microspheres can be observed (*arrows*). The arrowhead in *a* indicates the position of the growth cone. The position of the beads was confirmed by fluorescent images (*b* and *g*) of the same field. Bar, 10 μm.

injection (Fig. 2). Assuming that caged fluorescein-labeled tubulin is also incorporated homogeneously into all MTs, the observation that the injected cells showed no inhibition of the neurite extension rate suggests minimal effect of caged fluorescein-labeled tubulin on the mechanism of nerve growth. It is thus unlikely that modification of tubulin and photoactivation of MTs interfere with the native transport process of tubulin molecules. Moreover, the uniform incorporation of labeled tubulin eliminates the possibility that MTs are the form of active translocation but injected tubulin is selectively incorporated into dynamic but stationary MTs. This possibility arose from the report that stable and dynamic MTs coexist in the axon (3).

Second, it is also possible that the behavior of MTs might be different at different parts of the neurites. Indeed, the work of Reinsch et al. (46) reported the slower movement of photoactivated MTs in the proximal part of the *Xenopus* neurites. To eliminate this possibility, we generated fluorescent marks evenly on the proximal, middle, and distal parts of growing neurites. However, fluorescent zones were station-

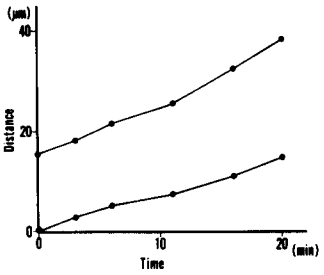

Figure 12. Movement of two fluorescent microspheres along the neurite shown in Fig. 11. The position of the two beads relative to the initial position of the more proximal bead was recorded. The beads translocated distally relative to the cell body. Furthermore, the inter-particle distance increased from 15 to 24 μm during the period of the 20-min observation.

ary regardless of the position of the activated zone, suggesting that MTs containing caged fluorescein-labeled tubulin in mouse neurons are stationary all along the length of the axon.

Third, the neurites of mouse DRG neurons may deviate from authentic axons and lack the normal system for active transport of the cytoskeletal proteins and mere diffusion functions to supply the protein required for in vitro neurite elongation at the tip. The difference of neurite branching pattern (namely, the neurites of mouse DRG neurons are highly branched and those of *Xenopus* are straight with few branches) may also lead to the inference that *Xenopus* neurites resemble authentic axons and mouse neurites do not, since the typical morphology of the axon is assumed to be a straight process with a few branches. However, we think this possibility is improbable since two to three days after plating, mouse neurons extend neurites of uniform diameter which can be longer than 2–3 mm (our own unpublished results). If tubulin molecules are moved only by diffusion, theoretical considerations have argued that neurite extension would become slower after the neurite length exceeds 1 mm (27). Furthermore, it is known that central axons (the dorsal root) of DRG neurons in situ send numerous collaterals onto the gray matter of the spinal cord (10) and this axon has an ability to transport cytoskeletal proteins (36). These reports indicate that the morphology of DRG neurons in culture resembles that in situ.

From these discussions, we conclude that the difference between mammalian and frog neurons is not derived from some technical artifacts, but reflects some biological characters of these two neuron types.

The Pattern of Neurite Growth Is Different between Mouse and Frog Neurons

We observed marked differences in the pattern of neurite extension between mouse and *Xenopus* neurons. They can be summarized as follows: (*a*) As stated previously, neurites of mouse DRG neurons are highly branched. In contrast, *Xenopus* neurons extend straight neurites with few branches. (*b*) Neurite growth rate of *Xenopus* neurons (60–250 μm/h) was faster than that of mouse DRG neurons (10–80 μm/h). (*c*) *Xenopus* neurites make contact with the culture substrate mainly at the growth cone and the neurite shaft is only loosely attached to, or even free from the substrate. In contrast, mouse neurites are sticky to the substrate and the neurite shaft does not change its direction when the growth cone moves laterally. These observations suggest that the tension generated by the *Xenopus* growth cone (6) would not be canceled by the cell-substrate contacts which seem to be very weak or absent in the *Xenopus* neurites. In combination with statement *b*, tension applied to the *Xenopus* neurite is higher than that applied to the mouse neurites. (*d*) Proximal part of the mouse DRG neurite did not change its position and shape during the increase in length at the distal part of the same neurite. A similar pattern of neurite growth is observed on rat sympathetic neurons and chick sensory neurons (5, 31). On the other hand, *Xenopus* neurites changed their shape rapidly and became progressively thinner as the growth cone moved away from the cell body (Fig. 6) and it was rather difficult to distinguish between net anterograde transport of the axonal structure and passive pulling by the growth cone. (*e*) Anterograde movement of the axon surface was observed in *Xenopus* neurons, which was not detected in mouse DRG neurons, chick sensory, and sympathetic neurons (4, 55). Statements *d* and *e* indicate that the growth pattern of *Xenopus* neurons is somewhat deviated from previous reports on mammalian or avian neurons in culture (4, 5, 31, 55).

When coupled with the discussion in the previous section, the sum of our efforts clearly demonstrates that there are major differences in the *Xenopus* and mammalian axons and suggests that the mechanisms for tubulin transport during extension of the frog and mammalian axons may be different. This then represents a conundrum, since a common mechanism for tubulin transport within vertebrate axons might seem a priori to be highly likely. To clarify this point, we will discuss the possible mechanism of tubulin transport on both neurons in the following section.

On the Mechanism of Tubulin Transport in the Axon

We have shown here that most MTs together with axon surface are stationary in the mouse neurites. Since net increase of the axonal structure distal to the photoactivated region was evidently observed (Figs. 3, 4, and 5), tubulin molecules necessary for the formation of new MT structure should be transported across the site of photoactivation. However, we did not detect such a fraction.

In *Xenopus* neurons, photoactivated tubulin molecules moved out from their initial position without significant spreading. Sliding of individual MTs with other MTs or other cytoskeletal components would result in broadening of the photoactivated region. Thus, this observation suggests that MTs are translocating en bloc and this implies that the bulk of cytoplasmic polymers in the axon does translocate. This is because MTs are the main cytoplasmic polymers in the neurites of *Xenopus* embryonal neurons in culture (8). In this sense, what structure is stationary in *Xenopus* neurites and against what structure MTs are translocated remain to be identified.

Because the simultaneous movement of photoactivated MTs and pieces of debris adhering to the neurites was frequently observed and the translocation rates of MTs and fluorescent beads were in the same range, it is reasonable to hypothesize that the two translocation phenomena are related. There could be two possible explanations for this relationship. One is that some components of membrane proteins and possibly the actin filaments underlying them are linked to moving MTs and active protrusion of MTs drags the former. In this case, the stationary components would be

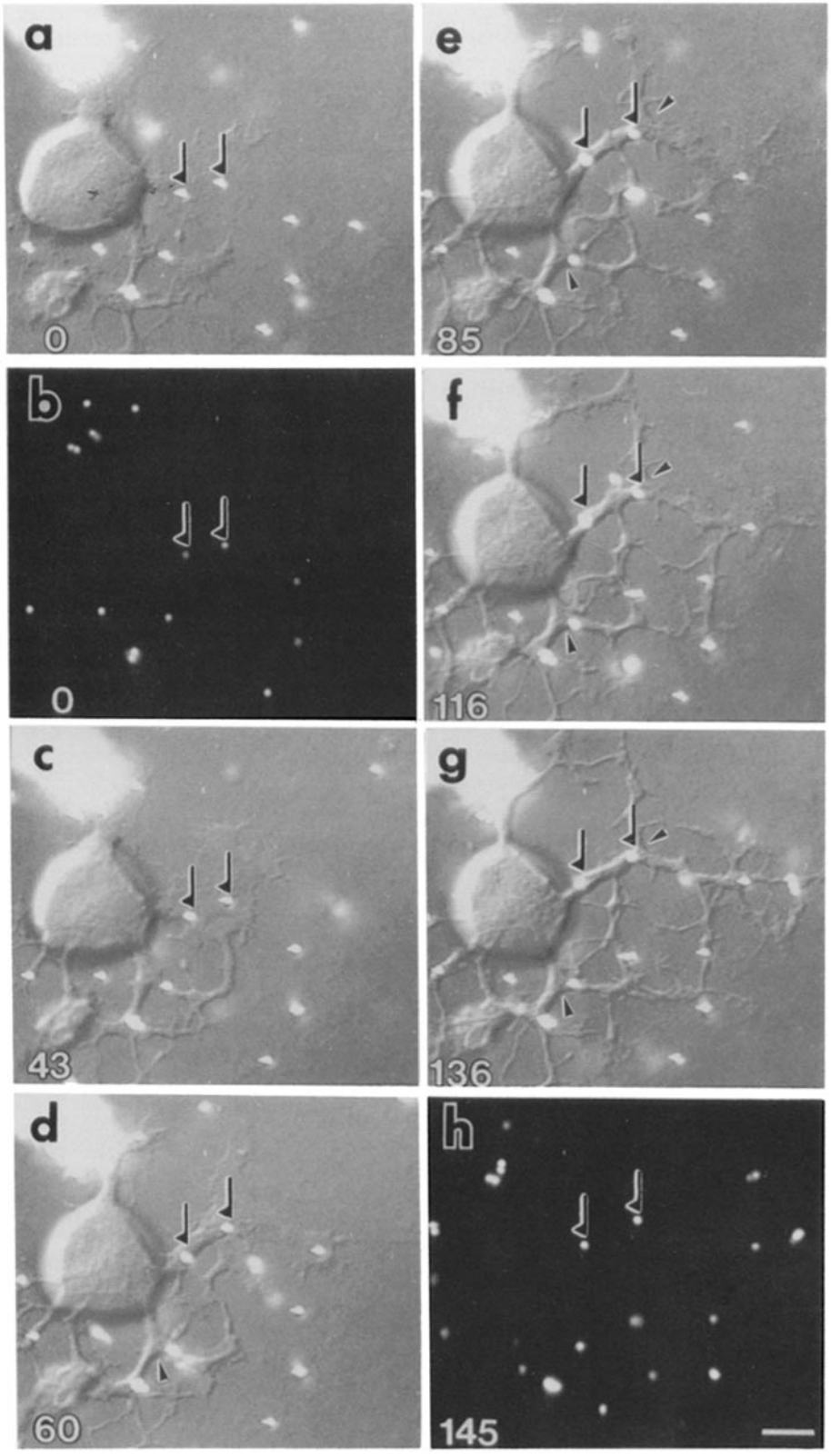

Figure 13. DIC images of a growing mouse DRG neuron. Two microspheres (*arrows*) on the dorsal surface of a large growth cone can be observed in *a*. During advancement of the growth cone (*a–g*), the microspheres remained in the same position, resulting in the formation of new neurites distal to the microspheres. The combined length of the newly formed neurites was ~50 μm. Arrowheads in (*d–g*) indicate the position of branching points, which were stationary throughout the observation. Times in minutes relative to *a* are given in the lower left-hand corner of each panel. The positions of the beads are also shown in the fluorescent images (*arrows* in *b* and *h*). Bar, 10 μm.

membrane lipids and membrane proteins not linked to moving MTs. The model basically fits with the classical hypothesis of the axonal transport which holds that the axonal cytoskeleton is extruded through the tunnel of the plasma membrane (7, 26, 27).

The other possibility is that the observed movement of the photoactivated zone and the adhering beads reports the movement of the whole axon structure. This model is illustrated in Fig. 14. It has been widely accepted that new surface is added at the growth cone in growth cone–mediated axonal elongation (4, 14, 45, 55). However, one of the major experimental bases that supports this statement is derived

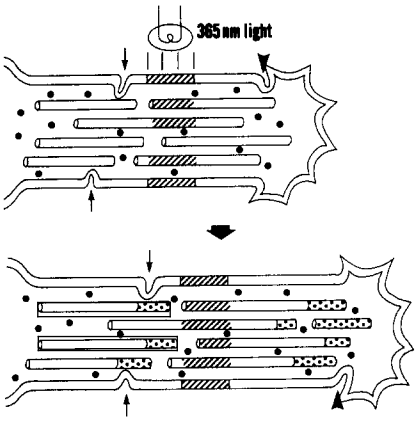

Figure 14. A model of MT translocation in neurites of *Xenopus* embryonal neurons. By irradiation of 365-nm light, small regions of MTs become fluorescent (▨, on cylinders). After photoactivation, insertion of a new membrane occurs at both the growth cone (*arrowheads*) and the neurite shaft (*small arrows*). Increase of new membrane behind the photoactivated region and pulling of the axon shaft by the growth cone result in the passive translocation of photoactivated MTs (▨, on cylinders) together with the corresponding region of the axon surface (▨, on membrane). During this period, tubulin molecules in a form of non-MT oligomer (●) are transported toward the neurite tip and assemble locally along the neurite (▨). This local assembly increases the net amount of MTs in the neurite.

from the observation that adhering beads do not change their position during nerve growth (4, 55). Since significant increase of interparticle distance along the neurite shaft occurs in *Xenopus* neurons, new membrane would be added at certain points along the neurite shaft (*small arrows* in Fig. 14) as well as at the growth cone (*arrowheads* in Fig. 14). So far, it is possible that the whole axonal structure distal to the membrane addition sites is dragged forward possibly by the tension generated at the rapidly advancing growth cones (6, 25, 55). Interestingly, as discussed previously, tension applied to *Xenopus* neurites is probably much higher than that applied to mouse neurites. In this case, no structure distal to the membrane addition sites is stationary and MTs are not actively protruded against other stationary structures within the axon but are passively dragged together with the other axonal components by the growth cone.

Further characterization of the movement of membrane components would be necessary to definitively test between the above two possibilities (28). However, the relatively large size of adhering beads and highly sticky nature of their surface suggest that the bead movement reports the behavior of large clusters of membrane proteins and does not reflect the movements of some minor membrane components. Thus we prefer the latter model, which seems to explain the bulk movement of membrane proteins more easily.

If the observed MT translocation in *Xenopus* neurons is because of passive pulling of the whole axon structure by the growth cone, the relation between the photoactivated MT movement and the mechanism of net tubulin increase in neurites should be re-evaluated. Mere pulling by the growth cone can not be the sole mechanism of nerve growth, since trailing of the cytoskeletal components behind the growth cone only elongates the neurite shape but does not contribute to the net increase of the neurite structure. Although the pattern of neurite growth of *Xenopus* neurons makes it difficult to precisely estimate the net increase of the axonal structure, it is apparent that net increase does occur (Figs. 6 and 9). In this sense, active transport mechanism distinct from the observed movement of photoactivated tubulin may exist in *Xenopus* neurons and we might not detect the fraction of tubulin molecules under active transport both in *Xenopus* and mouse neurons.

Assuming that in block translocation of photoactivated tubulin in *Xenopus* axons is a phenomenon related to drawing of the whole axon structure by the growth cone, the differential behavior of photoactivated MTs relative to the substrate might not be related to the profound difference of the mechanism of active tubulin transport in two neuron types. Rather, it is possible that the mechanism of MT turnover and active transport of tubulin molecules are identical in all neurons. Here it should be emphasized that, except the relative position of photoactivated MTs to the substrate, major features of MT behavior are very similar in both mouse and *Xenopus* neurons. Namely, fluorescence intensity of photoactivated zone decreased gradually with time, the length did not increase significantly, and the position did not change relative to the axon surface. These statements further reinforce the hypothesis that the mechanism of active tubulin transport is identical in all vertebrate neurons.

From all present data, the underlying mechanism of net tubulin transport into the axon is not yet clear. One possibility is that a very small number of MTs translocates in mouse and *Xenopus* axons. However, lack of translocating MTs across the photobleached zone in our previous photobleaching experiments on the mouse axon (43) suggests the absence of moving filaments, since our fluorescence detection system was able to detect splayed arrays of fluorescent filaments, possibly single fluorescein-labeled MTs, in the growth cone of mouse DRG neurons (our own unpublished results).

The other possibility is that tubulin dimer or a form of nonmicrotubule oligomer is the unit of transport (Fig. 14). Since it has been reported that tubulin molecules in the axon are largely assembled (37, 43), it is reasonable to hypothesize that the amount of nonmicrotubule fraction is small compared with MT polymers and fluorescent signals from this fraction could not be detected. Alternatively, gradual recovery or decay of fluorescence in photobleaching or photoactivation experiments might reflect some fraction of actively transported tubulin molecules. There have been reports suggesting the presence of translocating nonmicrotubule oligomers in the axon (51, 52). Our previous study of biotin–tubulin injection has shown that tubulin molecules introduced into the cell body of PC12 cells can be transported into the neurites as subunits or nonmicrotubule oligomers and incorporated into MTs locally (40). Progressive decrease of fluorescence in photoactivated zone and progressive increase of fluorescence in photobleached zone are common features of the neurites (30, 31, 43) and suggest that local assembly and disassembly of MTs should play an important role in the process of MT transport in the axon. These statements collectively indicate the possible function of transporting nonmicrotubule oligomers and their local assembly into MTs on net increase of MT structure in the axon. Future analysis on the nature of cytoskeletal proteins under active transport will elucidate the mechanism of nerve growth more clearly.

We thank Dr. K. Izutsu for the kind gift of PtK2 cells, Dr. D. W. Cleveland

for valuable comments on the manuscript, and Dojindo Laboratories for providing caged fluorescein.

This work was supported by a Special Grant-in-Aid for Scientific Research from the Ministry of Education, Science and Culture of Japan, and grants from RIKEN and the Naito Memorial Science Foundation to N. Hirokawa.

Received for publication 23 August 1991 and in revised form 26 December 1991.

References

1. Aletta, J. M., and L. A. Greene. 1988. Growth cone configuration and advance: a time-lapse study using video-enhanced differential interference contrast microscopy. *J. Neurosci.* 8:1425–1435.
2. Argiro, V., M. B. Bunge, and M. I. Johnson. 1984. Correlation between growth form and movement and their dependence on neuronal age. *J. Neurosci.* 4:3051–3062.
3. Baas, P., and M. M. Black. 1990. Individual microtubules in the axon consist of domains that differ in both composition and stability. *J. Cell Biol.* 111:495–509.
4. Bray, D. 1970. Surface movements during the growth of single explanted neurons. *Proc. Natl. Acad. Sci. USA.* 65:905–910.
5. Bray, D. 1973. Branching patterns of individual sympathetic neurons in culture. *J. Cell Biol.* 56:702–712.
6. Bray, D. 1987. Growth cones: do they pull or are they pushed? *Trends Neurosci.* 10:431–434.
7. Black, M. M., and R. J. Lasek. 1980. Slow components of axonal transport: two cytoskeletal networks. *J. Cell Biol.* 86:616–623.
8. Buchanan, J., Y. Sun, and M. Poo. 1989. Studies of nerve-muscle interactions in Xenopus cell culture: fine structure of early functional contacts. *J. Neurosci.* 9:1540–1554.
9. Caceres, A., and K. S. Kosik. 1990. Inhibition of neurite polarity by tau antisense oligonucleotides in primary cerebellar neurons. *Nature (Lond.).* 343:461–463.
10. Cajal, S. R. 1909. Histologie du systeme nerveux de l'homme et des vertebres. Maloine, Paris. 531 pp.
11. Daniels, M. P. 1973. Fine structural changes in neurons and nerve fibers associated with colchicine inhibition of nerve fiber formation in vitro. *J. Cell Biol.* 58:463–470.
12. Dinsmore, J. H., and F. Solomon. 1991. Inhibition of MAP2 expression effects both morphological and cell division phenotypes of neuronal differentiation. *Cell.* 64:817–826.
13. Dotti, C. G., C. A. Sullivan, and G. A. Banker. 1988. The establishment of polarity by hippocampal neurons in culture. *J. Neurosci.* 8:1451–1468.
14. Feldman, E. L., D. Axelrod, M. Schwartz, A. M. Heacock, and B. W. Agranoff. 1981. Studies on the localization of newly added membrane in growing neurites. *J. Neurobiol.* 12:591–598.
15. Gorbsky, G. J., P. J. Sammak, and G. G. Borisy. 1988. Microtubule dynamics and chromosome motion visualized in living anaphase cells. *J. Cell Biol.* 106:1185–1192.
16. Gurdon, J. B., and L. Wakefield. 1988. Microinjection of amphibian oocytes and eggs for the analysis of transcription. *In* Microinjection and Organelle Transplantation Techniques. J. E. Celis and A. Graessmann, editors. Academic Press, London. 269–299.
17. Hirokawa, N. 1982. Cross-linker system between neurofilaments, microtubules, and membrane organelles in frog axons revealed by the quick-freeze, deep-etching method. *J. Cell Biol.* 94:129–142.
18. Hirokawa, N. 1991. Molecular architecture and dynamics of the neuronal cytoskeleton. *In* The Neuronal Cytoskeleton. R. D. Burgoyne, editor. Wiley-Liss, New York. 5–74.
19. Hirokawa, N., M. A. Glicksman, and M. B. Willard. 1984. Organization of mammalian neurofilament polypeptides within the neuronal cytoskeleton. *J. Cell Biol.* 98:1523–1536.
20. Hoffman, P. N., and R. J. Lasek. 1975. The slow component of axonal transport. *J. Cell Biol.* 66:351–366.
21. Hollenbeck, P. J. 1989. The transport and assembly of the axonal cytoskeleton. *J. Cell Biol.* 108:223–227.
22. Kanai, Y., R. Takemura, T. Oshima, H. Mori, Y. Ihara, M. Yanagisawa, T. Masaki, and N. Hirokawa. 1989. Expression of multiple tau isoforms and microtubule bundle formation in fibroblasts transfected with a single tau cDNA. *J. Cell Biol.* 109:1173–1184.
23. Kidokoro, Y., M. J. Anderson, and R. Gruener. 1980. Changes in synaptic potential properties during acetylcholine receptor accumulation and neurospecific interactions in Xenopus nerve-muscle cell culture. *Dev. Biol.* 78:464–483.
24. Kristofferson, D., T. Mitchison, and M. Kirschner. 1986. Direct observation of steady-state microtubule dynamics. *J. Cell Biol.* 102:1007–1019.
25. Lamoureux, P., R. E. Buxbaum, and S. R. Heidemann. 1989. Direct evidence that growth cones pull. *Nature (Lond.).* 340:159–162.
26. Lasek, R. J. 1986. Polymer sliding in axons. *J. Cell Sci. Suppl.* 5:161–179.
27. Lasek, R. J. 1988. Studying the intrinsic determinants of neuronal form and function. *In* Intrinsic Determinants of Neuronal Form and Function. R. J. Lasek and M. M. Black, editors. Alan R. Liss Inc., New York. 3–58.
28. Lee, J., M. Gustafsson, D. E. Magnussen, and K. Jacobson. 1990. The direction of membrane lipid flow in locomoting polymorphonuclear leukocytes. *Science (Wash. DC).* 247:1229–1233.
29. Letourneau, P. C., and A. H. Ressler. 1984. Inhibition of neurite initiation and growth by taxol. *J. Cell Biol.* 98:1355–1362.
30. Lim, S. S., P. J. Sammak, and G. G. Borisy. 1989. Progressive and spatially differentiated stability of microtubules in developing neuronal cells. *J. Cell Biol.* 109:253–263.
31. Lim, S. S., K. J. Edson, P. C. Letourneau, and G. G. Borisy. 1990. A test of microtubule translocation during neurite elongation. *J. Cell Biol.* 111:123–130.
32. Lindsay, R. M. 1988. Nerve growth factors (NGF, BDNF) enhance axonal regeneration but are not required for survival of adult sensory neurons. *J. Neurosci.* 8:2394–2405.
33. McQuarrie, I. G., S. T. Brady, and R. J. Lasek. 1986. Diversity in the axonal transport of structural proteins: major difference between optic and spinal axons in the rat. *J. Neurosci.* 6:1593–1605.
34. Mitchison, T. J. 1989. Polewards microtubule flux in the mitotic spindle: evidence from photoactivation of fluorescence. *J. Cell Biol.* 109:637–652.
35. Mitchison, T. J., and M. W. Krischner. 1988. Cytoskeletal dynamics and nerve growth. *Neuron.* 1:761–772.
36. Mori, H., Y. Komiya, and M. Kurokawa. 1979. Slowly migrating axonal polypeptides: inequalities in their rate and amount of transport between two branches of bifurcating axons. *J. Cell Biol.* 82:174–184.
37. Morris, J. R., and R. J. Lasek. 1984. Monomer-polymer equilibria in the axon: direct measurement of tubulin and actin as polymer and monomer in axoplasm. *J. Cell Biol.* 98:2064–2076.
38. Newport, J., and M. Kirschner. 1982. A major developmental transition in early Xenopus embryos: 1. Characterization and timing of cellular changes at the midblastula stage. *Cell.* 30:675–686.
39. Nixon, R. A., and K. B., Logvinenko. 1986. Multiple fates of newly synthesized neurofilament proteins: evidence for a stationary neurofilament network distributed nonuniformly along axons of retinal ganglion cell neurons. *J. Cell Biol.* 102:647–659.
40. Okabe, S., and N. Hirokawa. 1988. Microtubule dynamics in nerve cells: analysis using microinjection of biotinylated tubulin into PC12 cells. *J. Cell Biol.* 107:651–664.
41. Okabe, S., and N. Hirokawa. 1989. Axonal transport. *Curr. Opin. Cell Biol.* 1:91–97.
42. Okabe, S., and N. Hirokawa. 1989. Incorporation and turnover of biotin-labeled actin microinjected into fibroblastic cells: an immunoelectron microscopic study. *J. Cell Biol.* 109:1581–1595.
43. Okabe, S., and N. Hirokawa. 1990. Turnover of fluorescently labelled tubulin and actin in the axon. *Nature (Lond.).* 343:479–482.
44. Okabe, S., and N. Hirokawa. 1991. Actin dynamics in growth cones. *J. Neurosci.* 11:1918–1929.
45. Pfenninger, K. H., and M. M. Pfenninger. 1981. Lectin labeling of sprouting neurons. 2. relative movement and appearance of glycoconjugates during plasmalemmal expansion. *J. Cell Biol.* 89:547–559.
46. Reinsch, S. S., T. J. Mitchison, and M. W. Kirschner. 1991. Microtubule polymer assembly and transport during axonal elongation. *J. Cell Biol.* 115:365–379.
47. Sammak, P. J., and G. G. Borisy. 1988. Direct observation of microtubule dynamics in living cells. *Nature (Lond.)* 332:742–746.
48. Sammak, P. J., G. J. Gorbsky, and G. G. Borisy. 1987. Microtubule dynamics in vivo; a test of mechanism of turnover. *J. Cell Biol.* 104:395–405.
49. Schulze, E., and M. Kirschner. 1986. Microtubule dynamics in interphase cells. *J. Cell Biol.* 102:1020–1031.
50. Tashiro, T., M. Kurokawa, and Y. Komiya. 1984. Two populations of axonally transported tubulin differentiated by their interactions with neurofilaments. *J. Neurochem.* 43:1220–1225.
51. Weisenberg, R. C., J. Flynn, B. Gao, S. Awodi, F. Skee, S. R. Goodman, and B. M. Riederer. 1987. Microtubule gelation-contraction: essential components and relation to slow axonal transport. *Science (Wash. DC).* 238:1119–1122.
52. Weisenberg, R. C., J. Flynn, B. Gao, and S. Awodi. 1988. Microtubule gelation-contraction in vitro and its relationship to component a of slow axonal transport. *Cell Motil. Cytoskeleton.* 10:331–340.
53. Willard, M. W., M. Cowan, and P. R. Vagelos. 1974. The polypeptide composition of intra-axonally transported proteins: evidence for four transport velocities. *Proc. Natl. Acad. Sci. USA.* 71:2183–2187.
54. Yamada, K. M., B. S. Spooner, and N. K. Wessells. 1971. Ultrastructure and function of growth cones and axons of cultured nerve cells. *J. Cell Biol.* 49:614–635.
55. Zheng, J., P. Lamoureux, V. Santiago, T. Dennerll, R. E. Buxbaum, and S. R. Heidemann. 1991. Tensile regulation of axonal elongation and initiation. *J. Neurosci.* 11:1117–1125.